Supporting Information

Anderson-type Polyoxometalate-based Complexes constructed from a new 'V'-like Bis-pyridine-bis-amide Ligand for Selective Adsorption of Organic Dyes and Detection of Cr(VI) and Fe(III) ions

Yue Zhang, Xiang Wang*, Yue Wang, Lei Li, Na Xu, XiuLi Wang*

†College of Chemistry and Materials Engineering, Bohai University, Liaoning Professional Technology Innovation Center of Liaoning Province for Conversion Materials of Solar Cell, Jinzhou 121013, P. R. China

Calculation of Capacity

Equation 1 was used to calculate the removal percentage of the dye.[1]

$$R\% = \left[\frac{A_0 - A_t}{A_0}\right] \times 100 \quad (1)$$

A_0 is the absorbance of the dye solution before the adsorption process; and A_t is the absorbance of the dye solution after the adsorption process.

Table S1 Crystallographic data of complexes **1**–**4**.

Complex	1	2	3	4
Empirical formula	C_{25} H_{42} Al Mo_6 N_4 O_{33} Zn	C_{25} H_{42} Cr Mo_6 N_4 O_{33} Zn	C_{25} H_{42} Al Mo_6 N_4 O_{33} Co	C_{25} H_{41} Cr Mo_6 N_4 O_{33} Co
Formula weight	1587.56	1618.63	1580.11	1611.18
Crystal system	Triclinic	Triclinic	Triclinic	Triclinic
Space group	P-1	P-1	P-1	P-1
a (Å)	7.0868(3)	7.0922(5)	7.0769(2)	7.0857(16)
b (Å)	16.8438(8)	16.8866(11)	16.8679(5)	16.920(4)
c (Å)	19.4954(10)	19.5181(13)	19.4622(6)	19.487(5)
α (°)	104.629(1)	104.652(1)	104.602(1)	104.599(5)
β (°)	95.856(1)	95.839(2)	96.266(1)	96.239(5)
γ (°)	99.846(1)	99.950(1)	99.599(1)	99.634(5)
V (Å 3)	2192.64(18)	2201.4(3)	2188.73(11)	2200.9(9)
Z	2	2	2	2
Dc (g cm^{-3})	2.405	2.442	2.398	2.431
μ (mm^{-1})	2.330	2.535	2.166	2.367
F (000)	1544	1578	1536	1570
Reflection collected	14808	13093	31457	16288
Unique reflections	9429	8053	10256	10769
parameters	653	653	665	655
Rint	0.039	0.0367	0.0245	0.035

GOF	0.984	1.005	1.090	0.994
$R_1{}^a[I \geqslant \alpha(I)]$	0.0425	0.0426	0.0525	0.0465
$wR_2{}^b$(all date)	0.0862	0.0934	0.1096	0.1021

$^aR_1 = \sum||Fo| - |Fc||/\sum|Fo|$; $^bwR2 = \Sigma[w(F_o^2-F_c^2)^2]/\Sigma[w(F_o^2)^2]^{1/2}$

Table S2 Selected bond distances (Å) and angles (°) of complexes **1**–**4.**

Complex 1			
Zn(1)-O(3)#3	2.221(4)	Zn(1)-O(2)	2.030(4)
Zn(1)-O(1W)	2.135(4)	Zn(1)-O(1)	2.131(4)
Zn(1)-O(2W)	2.058(4)	Zn(1)-N(1)	2.069(5)
O(1W)-Zn(1)-O(3)#3	91.20(18)	O(1)-Zn(1)-O(3)#3	169.66(16)
O(2W)-Zn(1)-O(3)#3	83.46(17)	O(1)-Zn(1)-O(1W)	99.13(18)
O(2W)-Zn(1)-O(1W)	168.32(17)	N(1)-Zn(1)-O(3)#3	90.35(17)
O(2W)-Zn(1)-O(1)	86.28(17)	N(1)-Zn(1)-O(1W)	90.29(18)
O(2W)-Zn(1)-N(1)	100.09(18)	N(1)-Zn(1)-O(1)	90.16(18)
O(2)-Zn(1)-O(3)#3	83.53(16)	O(2)-Zn(1)-O(1)	97.60(16)
O(2)-Zn(1)-O(1W)	80.19(16)	O(2)-Zn(1)-N(1)	168.54(19)
O(2)-Zn(1)-O(2W)	88.87(17)		
Symmetry codes for 1: #1 -x, -y+1, -z+2		#2 -x, -y, -z+1	#3 -x+1, -y+1, -z+2

Complex 2			
Zn(1)-O(3)#3	2.220(5)	Zn(1)-O(1)	2.125(5)
Zn(1)-O(2W)	2.062(5)	Zn(1)-O(1W)	2.141(5)
Zn(1)-O(2)	2.022(5)	Zn(1)-N(1)	2.061(6)
O(2W)-Zn(1)-O(3)#3	83.83(19)	N(1)-Zn(1)-O(3)#3	90.9(2)
O(2W)-Zn(1)-O(1)	86.1(2)	N(1)-Zn(1)-O(2W)	99.7(2)
O(2W)-Zn(1)-O(1W)	168.5(2)	N(1)-Zn(1)-O(1)	89.6(2)
O(2)-Zn(1)-O(3)#3	83.21(19)	N(1)-Zn(1)-O(1W)	90.5(2)
O(2)-Zn(1)-O(2W)	89.1(2)	O(1)-Zn(1)-O(3)#3	169.90(19)
O(2)-Zn(1)-O(1)	97.8(2)	O(1)-Zn(1)-O(1W)	99.4(2)
O(2)-Zn(1)-O(1W)	80.1(2)	O(1W)-Zn(1)-O(3)#3	90.7(2)
O(2)-Zn(1)-N(1)	168.9(2)		
Symmetry codes for 2: #1 -x, -y+2, -z+2		#2 -x, -y+1, -z+1	#3 -x+1, -y+2, -z+2

Complex 3			
Co(1)-O(3)#3	2.131(5)	Co(1)-O(1W)	2.111(5)
Co(1)-O(1)	2.035(5)	Co(1)-O(2)	2.124(5)
Co(1)-O(2W)	2.074(5)	Co(1)-N(1)	2.090(6)
O(1)-Co(1)-O(2W)	90.5(2)	N(1)-Co(1)-O(1W)	90.4(2)
O(1)-Co(1)-O(1W)	82.0(2)	N(1)-Co(1)-O(2)	88.1(2)
O(1)-Co(1)-O(2)	97.2(2)	O(2W)-Co(1)-N(1)	96.9(2)
O(1)-Co(1)-N(1)	171.3(2)	O(1W)-Co(1)-O(3)#3	91.9(2)
O(2W)-Co(1)-O(3)#3	84.62(19)	O(1W)-Co(1)-O(2)	98.9(2)

O(2W)-Co(1)-O(1W)	172.0(2)	O(2)-Co(1)-O(3)#3	169.2(2)
O(2W)-Co(1)-O(2)	84.8(2)	N(1)-Co(1)-O(3)#3	90.8(2)
Symmetry codes for **3**: #1 -x+2, -y+1, -z		#2 -x+2, -y+2, -z+1	#3 -x+1, -y+1, -z

Complex 4			
Co(1)-O(1W)	2.057(4)	Co(1)-O(1)	2.123(4)
Co(1)-O(2)#3	2.141(4)	Co(1)-O(2W)	2.113(4)
Co(1)-O(7)	2.032(4)	Co(1)-N(1)	2.093(5)
O(1W)-Co(1)-O(2)#3	84.70(16)	N(1)-Co(1)-O(2)#3	90.46(17)
O(1W)-Co(1)-O(1)	85.16(16)	N(1)-Co(1)-O(1)	88.30(18)
O(1W)-Co(1)-O(2W)	171.64(17)	N(1)-Co(1)-O(2W)	90.28(19)
O(1W)-Co(1)-N(1)	97.2(2)	O(7)-Co(1)-N(1)	171.48(19)
O(7)-Co(1)-O(1W)	89.71(18)	O(1)-Co(1)-O(2)#3	169.55(16)
O(7)-Co(1)-O(2)#3	85.15(16)	O(2W)-Co(1)-O(2)#3	91.47(18)
O(7)-Co(1)-O(1)	97.33(17)	O(2W)-Co(1)-O(1)	98.91(18)
O(7)-Co(1)-O(2W)	82.55(17)		
Symmetry codes for **4**: #1 -x, -y+2, -z+2		#2 -x, -y+1, -z+1	#3 x+1, y, z
#4 x-1, y, z			

Table S3 The charges and sizes of the selected organic dyes

	Cationic				**Anionic**
Name	**CV**	**MB**	**NR**	**RhB**	**MO**
Structural formula	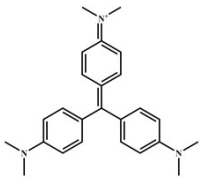	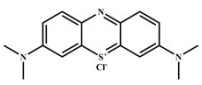	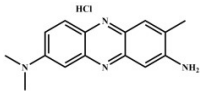	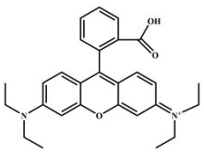	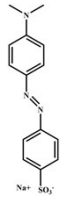
Charge	**+1**	**+1**	**+1**	**+1**	**-1**
x(Å)	**3.5**	**1.8**	**3.8**	**6.8**	**4.5**
y(Å)	**13.0**	**5.5**	**6.9**	**11.8**	**6.0**
z(Å)	**13.7**	**14.2**	**14.8**	**15.8**	**14.8**

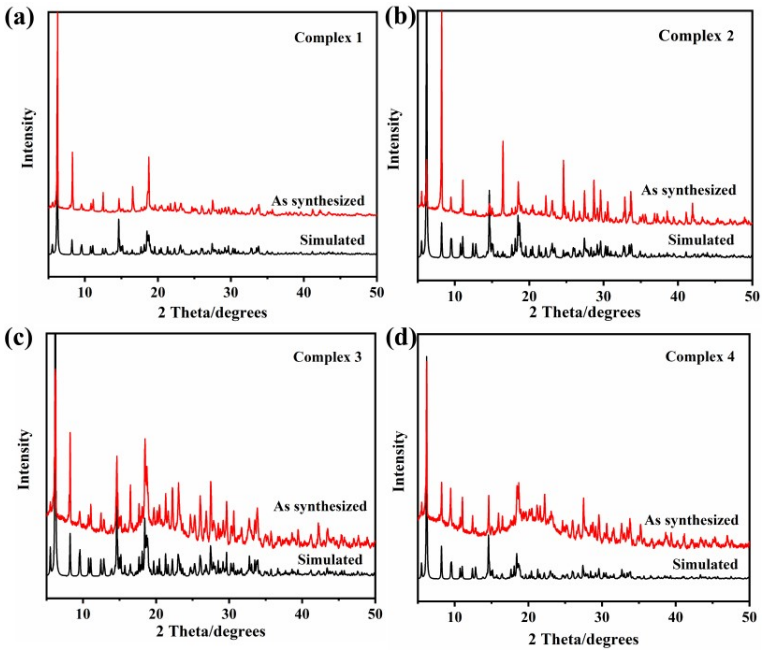

Fig. S1. The PXRD patterns of complexes **1**–**4**.

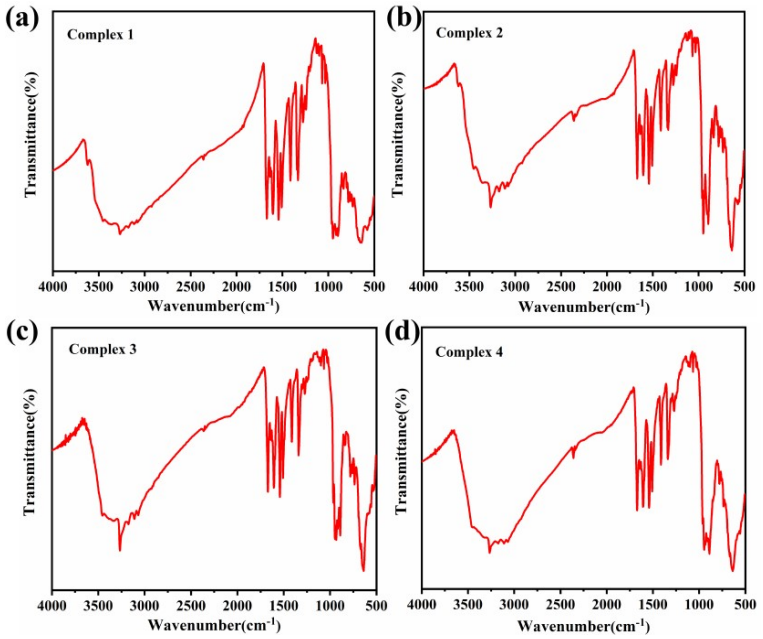

Fig. S2. The IR spectra of complexes **1**–**4**.

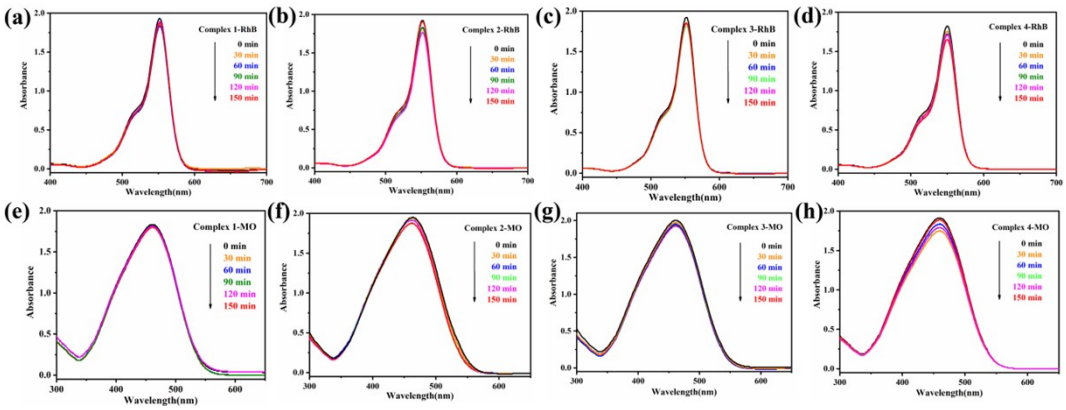

Fig. S3. UV/vis spectra of the **(a-d)** RhB and **(e-h)** MO in the presence of complexes **1**–**4**.

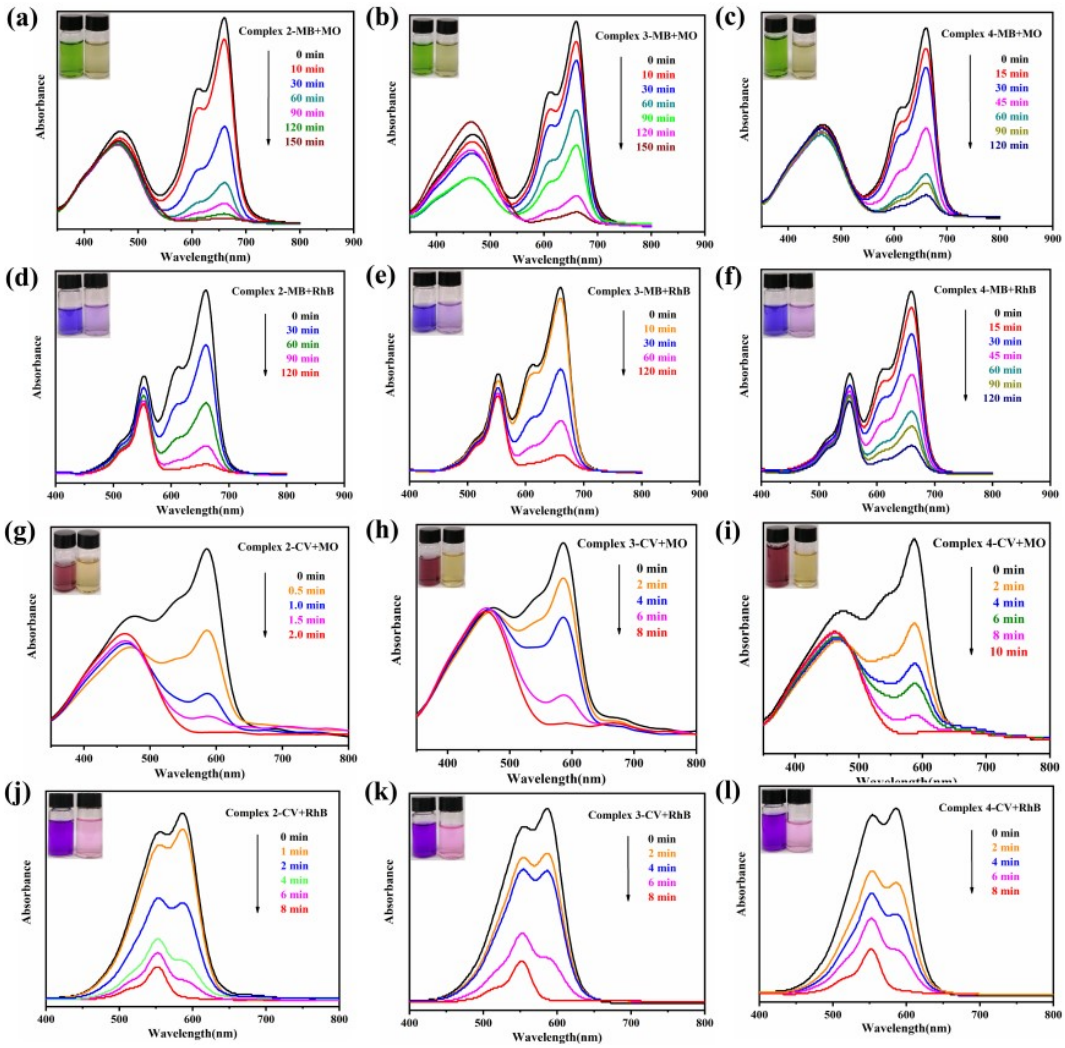

Fig. S4. UV/vis spectra of complexes **2**–**4** in the adsorption process of mixed dyes solution. The illustration showed the color change of the dye solutions before (left) and after (right) dye adsorption.

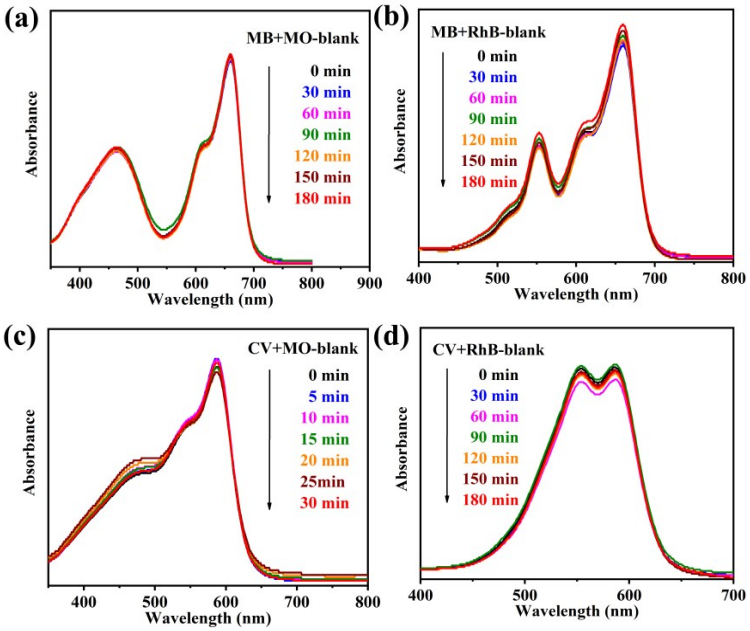

Fig. S5. UV/vis spectra of the binary mixed dyes without adsorbents. MB/MO **(a),** MB/ RhB **(b),** CV/MO **(c)** and CV/ RhB **(d)**.

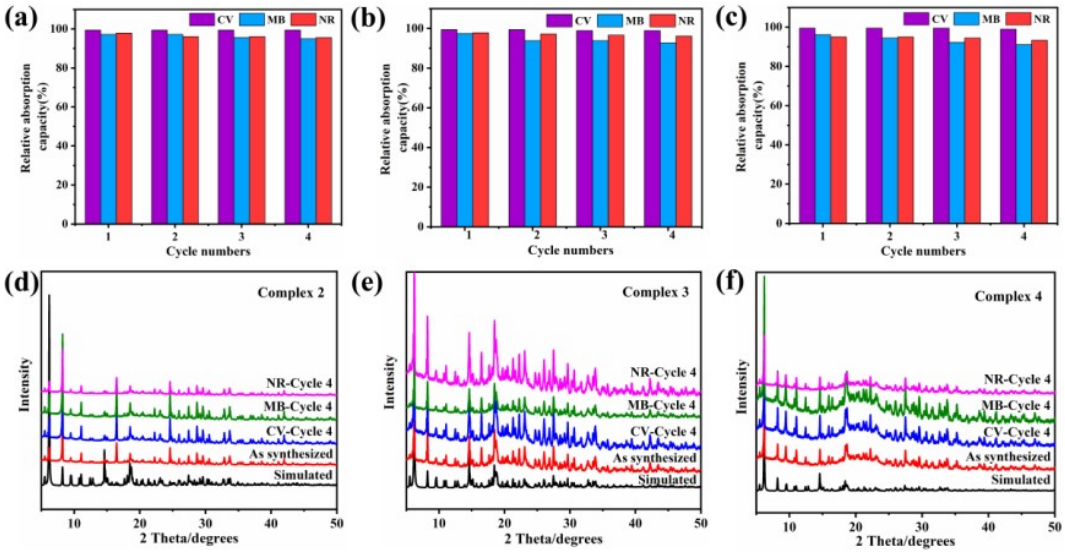

Fig. S6. (a-c) Four cycles of adsorption test of complexes **2**–**4** for CV, MB, and NR. **(b-f)** PXRD pattern of complexes **2**–**4** after four cycles of adsorption test.

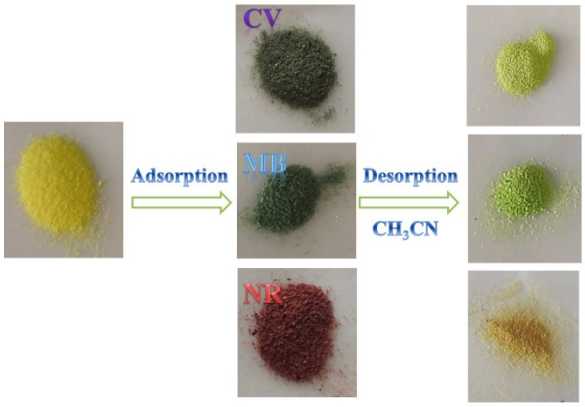

Fig. S7. The color change after adsorbing CV, MB, NR of **1** as adsorbent.

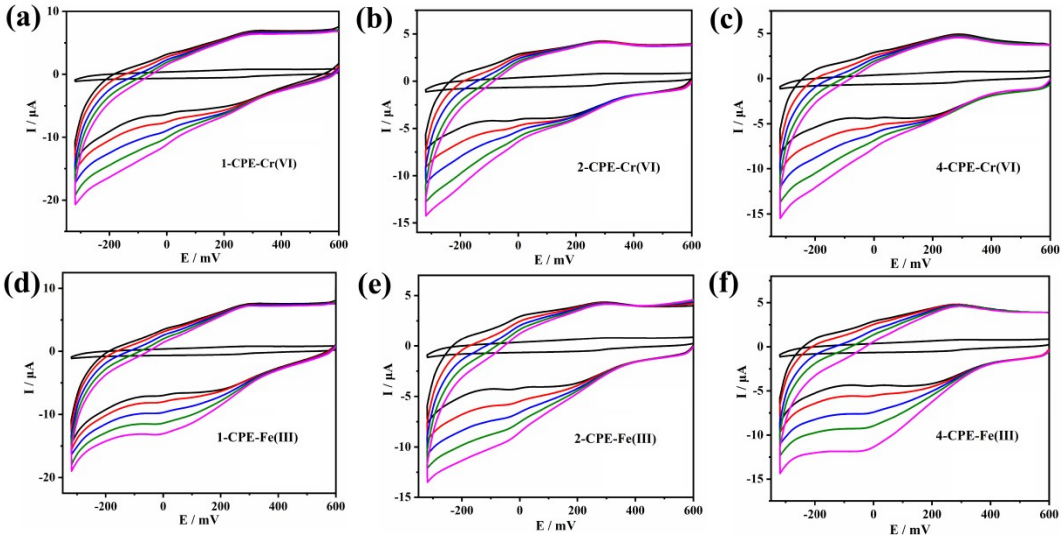

Fig. S8. (a-f) The cyclic voltammograms of **1**-, **2**-, **4**-CPE in electrolyte solution containing Cr(VI) ions and Fe(III) ions.

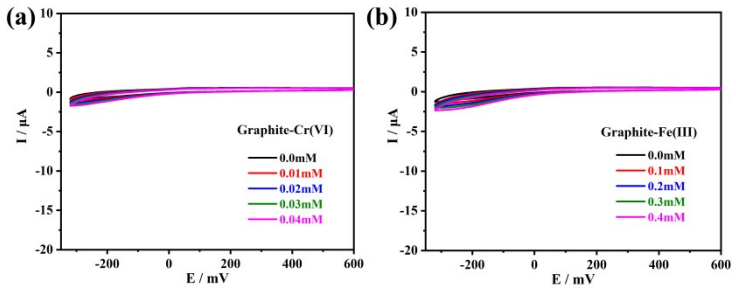

Fig. S9. The cyclic voltammograms of the bare-CPE in electrolyte solution containing Cr(VI) or Fe(III) ions.

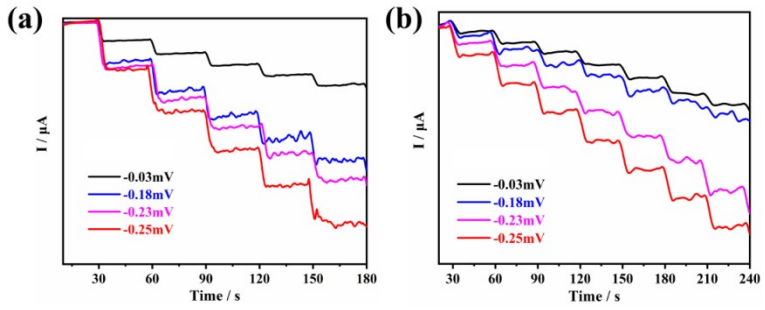

Fig. S10. The best potential of amperometric detection of **(a)** Cr(VI) ions and **(b)** Fe(III) ions for **3**-CPE.

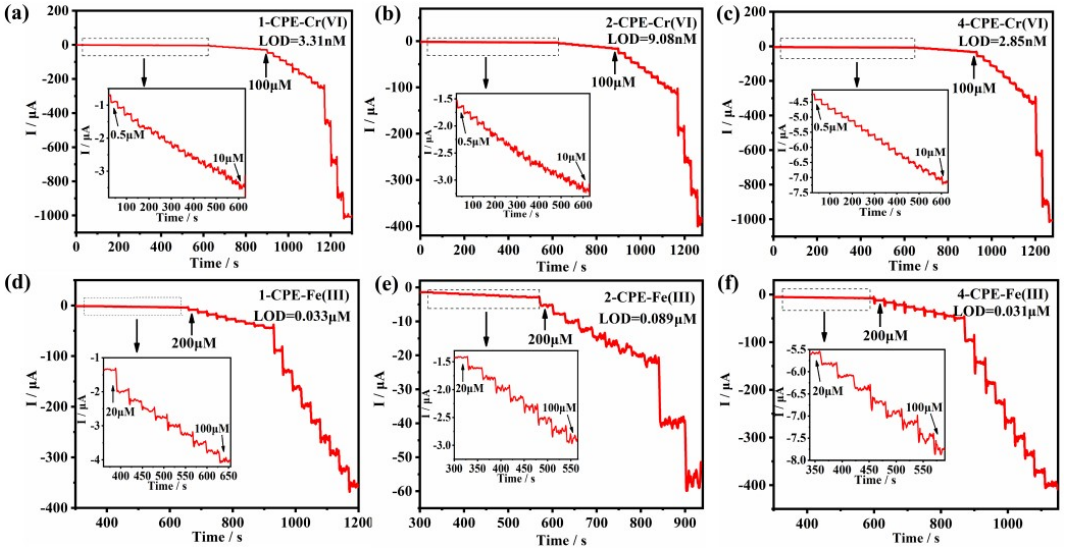

Fig. S11. Current response of **1**-, **2**-, **4**-CPE when **(a-c)** Cr(VI) ions and **(d-f)** Fe(III) ions are continuously added to electrolyte solution at -0.25 V.

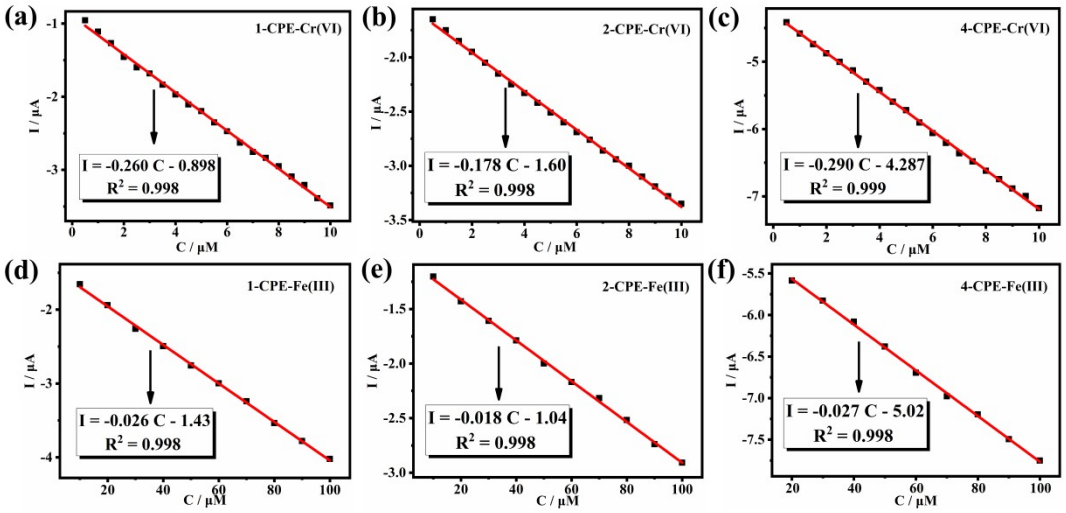

Fig. S12. Linear relationship between concentrations of Cr(VI), Fe(III) and redox currents of **1**-, **2**-, **4**-CPE.

Table S4 Comparison of complexes **1**–**4** with other reported sensors for the determination of Cr(VI).

Sensors' materials	Method	Sensitivity ($\mu A m M^{-1}$)	LOD (μM)	Reference
1	i-t	260	3.31×10^{-3}	this work
2	i-t	178	9.08×10^{-3}	this work
3	i-t	244	6.06×10^{-4}	this work
4	i-t	290	2.85×10^{-3}	this work
$[HC_5H_6N_2]_6\{M[Mo_6O_{12}(OH)_3(HPO_4)_3(H_2PO_4)]_2\}\cdot nH_2O$	i-t	224	0.026	2
$(H_2bpp)_6\{GdMo^V_2Mo^{VI}_{16}O_{49}(HPO_4)_3(PO_4)_3\}_2\cdot 11H_2O$	i-t	151	0.202	3
$(H_2bpp)_2[Na_4Fe(H_2O)_7][Fe(P_4Mo_6O_{31}H_6)_2]\cdot 2H_2O$	i-t	117	0.174	4
$[Cu^{II}_4(btmc)(ctcm)_4(\beta\text{-}Mo_8O_{26})]\cdot[\beta\text{-}Mo_8O_{26}]\cdot H_2O$	i-t	15.54	0.074	5
NiFe-NPs	i-t	35.5	0.01	6
$Ti/TiO_2NT/Au$	i-t	6.91	0.03	7

Table S5 Comparison of **1**–**4** with other reported sensors for the determination of Fe(III).

Sensors' materials	Method	Sensitivity ($\mu A m M^{-1}$)	LOD (μM)	Reference
1	i-t	26	0.033	this work
2	i-t	18	0.089	this work
3	i-t	77	0.019	this work
4	i-t	27	0.031	this work
$\{[H_2N(CH_3)_2]][Co_2(BDC)SO_4F(H_2O)]\}$	CV	-	0.1	8
SMS-2	DPV	7.33×10^{-4}	0.93	9
PEDOT−DFA nanowires	CV	-	0.01	10

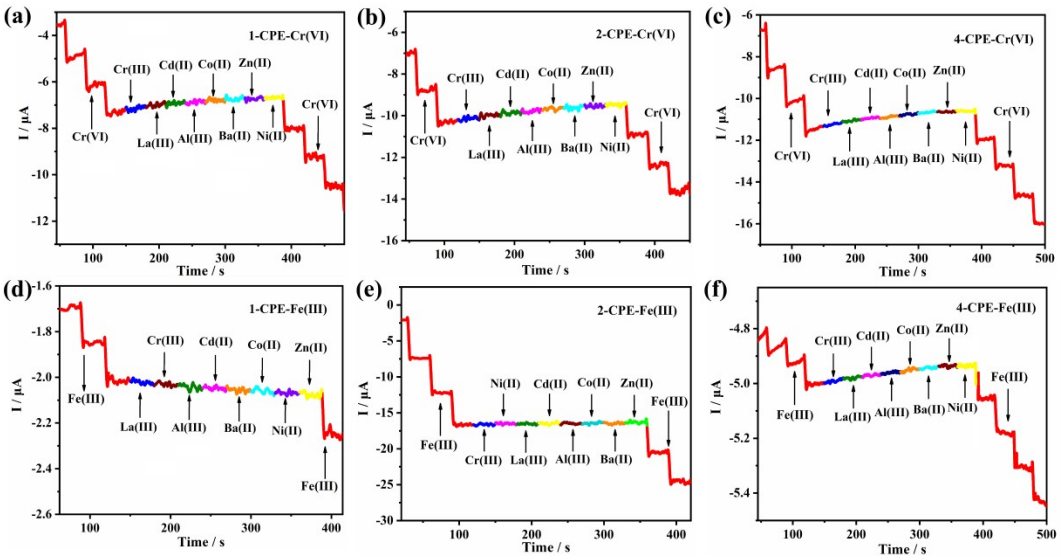

Fig. S13. Current response of **1**-, **2**-, **4**-CPE contains Cr(VI) **(a-c)** and Fe(III) ions **(d-f)** with continuous addition of various metal ions (100 μM Cr^{3+}, Al^{3+}, Cd^{2+}, La^{3+}, Ba^{2+}, Co^{2+}, Ni^{2+}, Zn^{2+}).

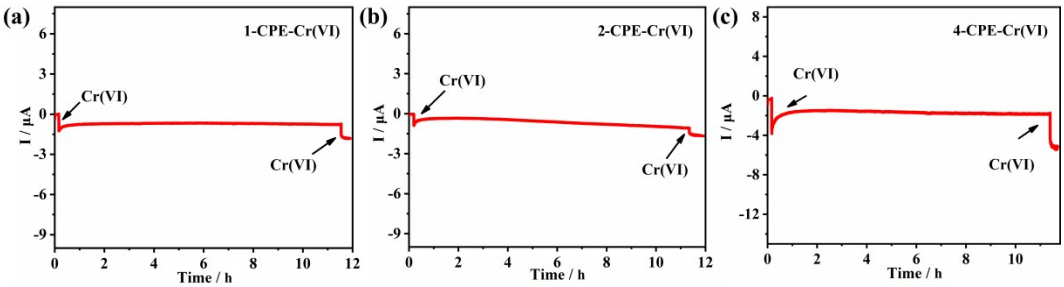

Fig. S14. The stabilities of **1**, **2**, **4**-CPE to the ampere response of 10 μM Cr(VI) for 10 h.

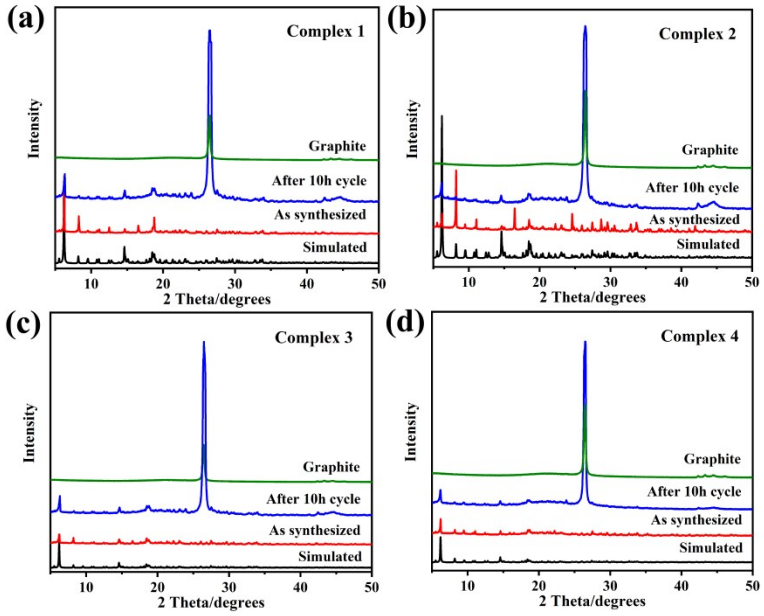

Fig. S15. The PXRD of **1**–**4**-CPEs after working 10 h.

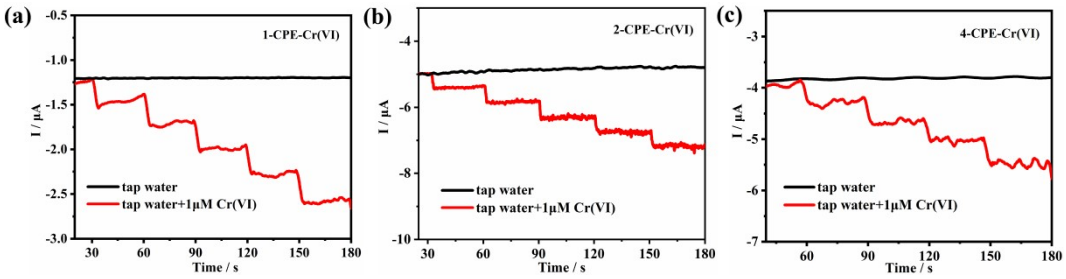

Fig. S16. Current response of **1**-, **2**-, **4**-CPE to detects trace Cr(VI) in tap water samples.

Reference

1. J. Wang, Y. S. Liu, X. Y. Guo, H. Q. Qu, R. Chang and J. Ma, Efficient Adsorption of Dyes Using Polyethyleneimine-Modified NH_2-MIL-101(Al) and its Sustainable Application as a Flame Retardant for an Epoxy Resin, *ACS Omega*, 2020, **5**, 32286-32294.
2. Y. L. Wang, Y. Y. Ma, Q Zhao, L. Hou and Z. G. Han, Polyoxometalate-Based Crystalline Catalytic Materials for Efficient Electrochemical Detection of Cr(VI), *Sensors and Actuators B:Chemical*, 2020, **305**, 127469-127489.
3. J. Q. Niu, Y. Y. Ma, X. Xin, Z. G. Han, Rare-Earth Ion Encapsulated Basket-like $\{GdP_6Mo^{V}_2Mo^{VI}_{16}O_{73}\}$ Cage as Efficient Electrochemical Sensor and Fluorescent Probe for Cr(VI), *Crystal Growth & Design*, 2020, **20**, 3584-3589.
4. X. Xin, N. Hu, Y. Y. Ma, Y. L. Wang, L. Hou, H. Zhang and Z. G. Han. Polyoxometalate-based crystalline materials as a highly sensitive electrochemical sensor for detecting trace Cr(VI), *Dalton Transactions*, 2020, **49**, 4570-4577.
5. C. Wang, J. Ying, H. C. Mou. A. X. Tian and X. L. Wang, Multi-functional Photoelectric Sensors based on A Series of Isopolymolybdate-based Compounds for Detecting Different Ions, *Inorganic Chemistry Frontiers*, 2020, **7**, 3882-3894.
6. J. Liu, D. Yu, L. Ji, Z. Xin and W. Wang, Highly sensitive detection of Cr(VI) in ground water by bimetallic NiFe nanoparticles, *Analytical Methods*, 2017, **9**, 1031-1037.
7. W. Jin, G. S. Wu and A. C. Chen, Sensitive and selective electrochemical detection of chromium(VI) based on gold nanoparticle-decorated titania nanotube arrays, *Analyst*, 2013, **139**, 235-241.
8. L. Y. Pang, P. Wang, J. J. Gao, Y. Wen, H. Liu, An active metal-organic anion framework with highly exposed SO_4^{2-} on {001} facets for the enhanced electrochemical detection of trace Fe^{3+}, *Journal of Electroanalytical Chemistry*, 2019, **836**, 85-93.

9. S. K. Mittal, S. Rana, N. Kaurand C. E. Banks. Voltammetric Method for Fe (III) in Blood Serum using Screen Printed Electrode modified with a Schiff Base ionophore, *Analyst*, 2018, **143**, 2851-2861.
10. L. R. Kindra, C. J. Eggers, A. T. Liu, K. Mendoza, J. Mendoza, A. R. Klein Myers, R. M. Penner, Lithographically Patterned PEDOT Nanowires for the Detection of Iron(III) with Nanomolar Sensitivity, *Analytical Chemistry*, 2015, **87**, 11492-500.